AGU PUBLICATIONS

Geophysical Research Letters

RESEARCH LETTER
10.1002/2016GL068835

Key Points:
- We were able to estimate latent heating and vertical velocity profiles in the ITCZ directly from TRMM PR precipitation profiles
- The fall ITCZ circulation has dual cells, but the double ITCZs in spring have primarily single deep cells on their poleward flanks
- Reanalyses and satellite retrievals are not reliable to characterize the vertical structure of the vertical circulation in the ITCZ

Supporting Information:
- Supporting Information S1

Correspondence to:
L. Huaman,
lidiana.huaman@gmail.com

Citation:
Huaman, L., and K. Takahashi (2016), The vertical structure of the eastern Pacific ITCZs and associated circulation using the TRMM Precipitation Radar and in situ data, *Geophys. Res. Lett.*, *43*, 8230–8239, doi:10.1002/2016GL068835.

Received 23 MAR 2016
Accepted 15 JUL 2016
Accepted article online 18 JUL 2016
Published online 14 AUG 2016

The vertical structure of the eastern Pacific ITCZs and associated circulation using the TRMM Precipitation Radar and in situ data

L. Huaman[1,2] and K. Takahashi[1]

[1] Instituto Geofísico del Perú, Lima, Peru, [2] Departamento de Ingeniería Ambiental, Física y Meteorología, Universidad Nacional Agraria La Molina, Lima, Peru

Abstract The atmospheric circulation associated with the eastern Pacific single and double ITCZs, particularly its vertical structure, is little known due to the sparce observations. Using precipitation profiles from the Tropical Rainfall Measure Mission (TRMM) Precipitation Radar, with approximations to the liquid water and energy budget equations, we estimated vertical profiles of latent heating and vertical velocity in the far eastern Pacific (95°W–85°W) ITCZs in the 800–730 hPa layer. We combined this with Eastern Pacific Investigation of Climate campaign (EPIC2001) and other in situ data to produce a preliminary characterization of the meridional-vertical circulation. We found evidence of a double-cell structure in boreal fall between the ITCZ and the equator, with both shallow and upper level peaks in vertical velocity. In spring, the flow poleward of the two ITCZs has a single-cell structure, although around the equator it shows some hints of the double cells. Reanalysis and satellite-based data are shown to be unreliable for describing the vertical structure of the circulation.

1. Introduction

The eastern Pacific presents challenges to climate models, particularly the double ITCZ bias [*Mechoso et al.*, 1995; *Flato et al.*, 2013; *Zhang et al.*, 2015]. In nature, the ITCZ is primarily north of the equator (e.g., Figure 1a), but it presents double ITCZs in boreal spring [*Zhang*, 2001] (Figure 1b), albeit with much weaker precipitation than the models. During extreme El Niño events, the cold tongue disappeared and a single strong ITCZ was seen south of the equator [*Lietzke et al.*, 2001; *Gu et al.*, 2005].

Air-sea coupling plays a crucial role in the far eastern Pacific climate [e.g., *Xie and Philander*, 1994; *Takahashi and Battisti*, 2007], where the ITCZs, the northeast Pacific warm pool and the Costa Rica Dome, the gap winds from Central America, [*Xie et al.*, 2005], the equatorial cold tongue [*Zhang*, 2001], and the southeast Pacific coastal upwelling and stratus clouds [*Philander et al.*, 1996; *Ma et al.*, 1996] interact, potentially affecting the climate toward the west [*Xie*, 1996; *Takahashi and Battisti*, 2007].

Although air-sea coupling is important for the double ITCZ bias [*Lin*, 2007; *de Szoeke and Xie*, 2008], this bias could be originating in the atmospheric models [*Lin*, 2007], particularly through the relation between precipitation and large-scale circulation [*Bellucci et al.*, 2010; *Oueslati and Bellon*, 2015]. However, despite observational efforts such as the EPIC project [*Cronin et al.*, 2002; *Raymond et al.*, 2004], our knowledge of the fundamental characteristics of the circulation in this region remains limited, particularly with respect to the vertical structure of latent heating in the ITCZs, with apparent discrepancies between Tropical Rainfall Measure Mission (TRMM)-based retrievals, which indicate a top heavy profile in the Northern Hemisphere (NH) ITCZ [*Schumacher et al.*, 2004], with in situ observations that support the existence of a shallow meridional overturning circulation in this region (e.g., Eastern Pacific Investigation of Climate campaign (EPIC2001) [*Zhang et al.*, 2004, 2008; *Nolan et al.*, 2007] and the First Global Atmospheric Research Program Global Experiment [*Yin and Albrecht*, 2000]), while atmospheric reanalysis data indicate a predominantly bottom heavy profile, with shallow maximum ascent [*Back and Bretherton*, 2006, 2009; *Handlos and Back*, 2014]. Reanalysis data, however, do not completely reproduce the observed characteristics in the ITCZ region [*Hastenrath*, 2002], while TRMM-based retrieval algorithms use vertical structures from look-up tables [*Tao et al.*, 2001, 2006, 2010; *Shige et al.*, 2004, 2007; *Kodama et al.*, 2009]. On the other hand, there is very little work on the double ITCZ in spring, which is when models have the worst biases [*Zhang et al.*, 2015].

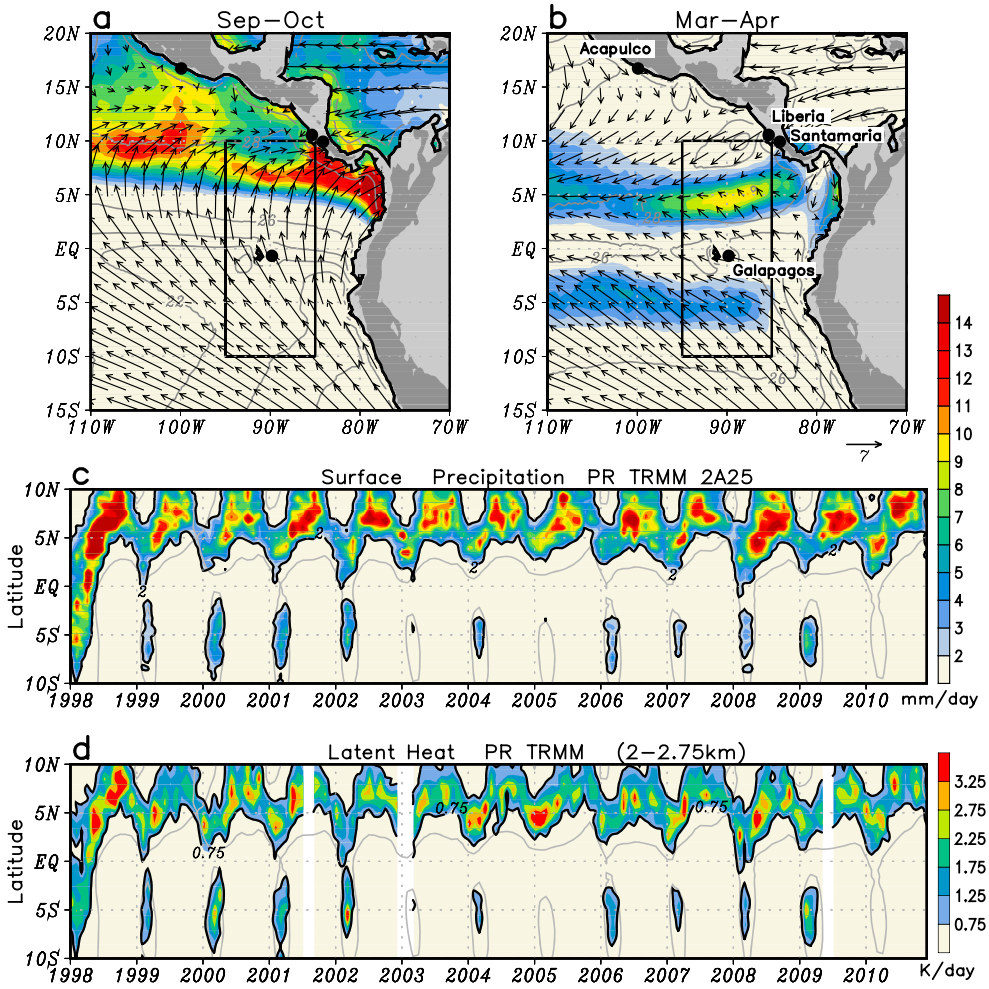

Figure 1. Mean 2001–2009 precipitation from PR-TRMM 3B43 in shaded, sea surface temperature from TMI TRMM in contours and surface wind from QuikSCAT in (a) September–October and (b) March–April. Dark shades denote topography greater than 500 m. Time-latitude diagrams (average 95°W–85°W) of (c) surface precipitation from PR-TRMM 2A25 in mm d^{-1} and (d) mean 2–2.75 km latent heat in K d^{-1}.

In this study we sketch a synthetic picture of the climatological meridional circulation in the far eastern Pacific, for which we revisit existing observations, complemented with the first estimate of monthly mean vertical profiles of latent heating and vertical air velocity in the ITCZs directly calculated from the TRMM Precipitation Radar (PR) precipitation profiles.

2. Data and Methodology

Our study region is the far eastern Pacific (95°W–85°W; 10°S–10°N; Figure 1a), which includes the eastern-most part of the double ITCZs and the equatorial cold tongue. In addition to the TRMM PR data, within this domain we have the in situ observations from the EPIC2001 campaign, radiosoundings, the wind profiler radar on the Galápagos island, and the 95°W Tropical Atmosphere-Ocean (TAO) mooring line.

2.1. Reanalysis Data

We used atmospheric data from the ERA-Interim [*Dee et al.*, 2011] and National Centers for Environmental Prediction (NCEP)/National Center for Atmospheric Research (NCAR) reanalysis [*Kalnay et al.*, 1996; *Kistler et al.*, 2001], which are based on global atmospheric models and data assimilation systems. It should be noted that variables associated with precipitation are not well constrained by this process [*Kalnay et al.*, 1996], particularly in the tropics [*Janowiak et al.*, 1998; *Wu and Xie*, 2003]. We used monthly data on pressure levels, provided on 0.5° × 0.5° and 2.5° × 2.5° grids, respectively. The latter was bilinearly interpolated to the former's grid.

2.2. Vertical Profiles From TRMM PR

We used precipitation rate (P) profiles from the Tropical Rainfall Measure Mission (TRMM) Precipitation Radar (PR) [*Kummerow et al.*, 1998]; product 2A25 V7 [*JAXA and NASA*, 2011], using swaths (220 km wide) with data in our domain during 1998–2010. The nominal vertical resolution is 0.25 km at the 0.25–20 km altitudes. The precipitation rate is calibrated for rain and cannot be quantitatively used for solid precipitation [*Iguchi et al.*, 2000]. There is a theoretical sensitivity limit of 0.4 mm h^{-1}, so the precipitation profiles have artificial discontinuities near the storm tops, which are intensified near the melting layer at 5 km due to the difference in the refractive index of water and ice [*Short and Nakamura*, 2000]. Thus, we limited the analysis to altitudes below 3 km, only considering profiles with storm tops (highest level with nonzero reflectivity) above 3 km. This excludes around 45% of shallow profiles, verified to only contribute 4% of total precipitation. Additionally, since surface clutter [*Iguchi et al.*, 2000] could bias the near-surface results toward heavier rainfall, we limited the analysis to above 1.75 km, the lowest level with over 60% of complete data. Summarizing, precipitation was considered every 0.25 km between 1.75 and 3 km.

TRMM 2A25 version 5 agreed well with mooring data but underestimated the accumulated near-surface precipitation by up to 40% on monthly and seasonal scales [*Serra and McPhaden*, 2003], while version 6 underestimated convective rain rates even more [*Tao et al.*, 2010]. Comparing version 7 with data from TAO moorings along 95°W (8°N, equator and 5°S) shows that it only underestimates the total rainfall by 11% in the NH ITCZ (8°N) and overestimated it by less than 10% in the Southern Hemisphere (SH) ITCZ (5°S) and the equator during boreal winter/spring (Figure S1 in the supporting information).

To calculate the large-scale monthly mean net condensation, we can neglect the horizontal transport and storage terms in the liquid water budget, so we have a balance between net condensation (C) and vertical divergence of the vertical flux of liquid water (i.e., P, positive toward the surface), i.e., $C=-\partial P/\partial z$. Derivatives were estimated using centered vertical differences, so the results are available at the 2, 2.25, 2.5, and 2.75 km levels (approximately 802, 779, 756, and 734 hPa, respectively, based on mean ERA-Interim geopotential height over our domain). Latent heat (LH) profiles were estimated from $\mathrm{LH}=CL_v(c_p\rho)^{-1}$ in K/d, where L_v is the latent heat of vaporization, c_p is the specific heat of air at constant pressure, and ρ is the air density.

To estimate vertical pressure velocity (ω), we assumed that vertical advection of potential temperature balances LH (i.e., neglecting horizontal advection, turbulent diffusion, and radiative tendencies [*Houze*, 1989]). Thus, $\omega\approx\mathrm{LH}(\partial\ln\theta/\partial p)^{-1}T^{-1}$, where θ is the potential temperature and T the air temperature. The values for θ, T, and ρ were obtained from ERA-Interim.

The data were averaged zonally within 0.5° latitude bins (with approximately 37 profiles per bin per month). Additionally, we calculated averages within the ITCZ by considering the latitude ranges in which the monthly zonal mean surface precipitation values from TRMM 2A25 exceeded 2 mm d^{-1}, both in the NH and SH ITCZs.

To the best of our knowledge, this is the first attempt to directly use the TRMM PR precipitation rate profiles to estimate latent heating. Our method is fundamentally different from the TRMM-based algorithms (section 2.4) that use prescribed profiles rather than measuring them.

2.3. EPIC2001

We used meridional wind profiles from dropsondes from eight flights during EPIC2001 [*Raymond et al.*, 2004; *de Szoeke et al.*, 2005] along 95°W (0°–12°N, 1000–500 hPa) during September–October 2001 around 20 UTC (near the peak in the diurnal cycle of convection [*Bain et al.*, 2010]).

Vertical velocity was estimated by approximating $\partial\omega/\partial p\approx-\partial v/\partial y$ (i.e., assuming $|\partial v/\partial y|\gg|\partial u/\partial x|$) and taking $\omega=0$ at the lowest level. This approximation, as well as the representativeness of the eight flights, was approximately verified by sampling ERA-Interim reanalysis in the same way and comparing with its actual values of ω.

We produced a rough estimate of the vertical velocity profile above 500 hPa using the following constraints. We estimated the latent heat profile between cloud base at 950 hPa (approximately the lifting condensation level in the EPIC2001 data set) and 500 hPa with the same method as for TRMM PR. Since the total column-integrated LH is proportional to the net surface precipitation (P) on monthly scales, we used P and the LH from EPIC2001 to estimate the layer-integrated LH above 500 hPa. We then assumed that the vertical profile in this layer is a cubic function of pressure so that LH (1) is continuous at 500 hPa, (2) is zero at 200 hPa, (3) has its maximum at 400 hPa [*Schumacher et al.*, 2004], and (4) is energetically balanced so its vertically integral

between 500 and 200 hPa is given by $(L_v P)c_p^{-1} - \int_{500\text{hPa}}^{950\text{hPa}} \text{LH} g^{-1} dp$. Finally, the vertical velocity profile above 500 hPa was estimated as before.

2.4. TRMM-Based Latent Heat Retrievals

We compared our results with results from algorithms based partly on TRMM PR: Convective-Stratiform Heating (CSH6 and CSH7 based in TRMM version 6 and 7, respectively [*Tao et al.*, 2001, 2006, 2010]), Spectral Latent Heating (SLH) [*Shige et al.*, 2004, 2007], and PR Heating (PRH) [*Satoh et al.*, 2001; *Kodama et al.*, 2009]. These TRMM-based algorithms use profiles from look-up tables and/or TRMM convective and stratiform classification to provide vertical profiles of latent heat, except CSH6, which provides the sum of latent heating, radiative tendencies and turbulent diffusion profiles, although LH is the largest component in the ITCZ. The profile shapes were obtained from field campaigns and cloud-resolving models, corresponding to deep-convective conditions, not necessarily representative of the eastern Pacific.

2.5. Other Data

We also used the TRMM 3B43 version 7 monthly surface precipitation, which is a blend of geostationary satellite data calibrated with microwave and radar data from TRMM [*Huffman et al.*, 2007], as well as the TRMM TMI version 4 monthly SST [*Gentemann et al.*, 2004]. We also considered precipitation from the 95°W TAO mooring line.

For winds, we used the QuikSCAT surface climatology (2000–2009) [*Ricciardulli and Wentz*, 2011], radiosoundings at three stations during 1998–2015 (Acapulco (16.83°N, 99.96°W, 3 meters above sea level (masl)), Juan Santamaria International Airport (9.98°S, 84.21°W, 932 masl) and San Cristobal, Galápagos (0.43°S 89.60°W, 6 masl)), pilot balloons in Liberia (April 1997–1998, 10.63°N, 85.44°W, 80 masl), and the EPIC ship-based radiosoundings along 95°W (8°S–10°N, April and November 1999 and 2001) [*Cronin et al.*, 2002]. We also analyzed the monthly mean meridional wind profiles from the 915 MHz wind profiler radar (high mode) in the Galápagos Islands (1994–2006; 0.9 °S, 89.6°W, 8 masl [*Hartten and Gage*, 2000]).

3. Results

3.1. Climatological Vertical Motion in the ITCZs

The monthly and latitudinal variability in surface P (Figure 1c) and our 2–2.75 km LH (Figure 1d) are highly correlated ($r \approx 0.68$). In 1998–2010, the double ITCZ was typically observed between February and April, and to a lesser extent, in May, with the SH branch between 8°S and 3°S (Figures 1b–1d and S1), with the exception of 2005 and 2010. During the extreme El Niño event in 1998, a strong single ITCZ was present across the equator (Figures 1c and 1d) [*Halpern and Hung*, 2001; *Zhang*, 2001]. On average, the NH ITCZ extends between 1°N and 7°N in spring, peaking between 4°N and 5°N, while in fall (September–October) it is located between 4.5°N and the coast near 16°N, peaking around 7°N (Figure 1a). Our domain edge coincides with the minimum in precipitation at 10°N, proposed to be associated with a zonal minimum in SST and the Costa Rica dome [*Xie et al.*, 2005] (Figure 1a).

The climatological values and the correlation between the interannual anomalies of ω in the ITCZs show good agreement of our data with CSH6 at the common altitudes and, to a lesser extent, with SLH but not with CSH7 and PRH (Figure 2), whereas both reanalyses overestimate the climatological values by a factor of 2–3. The seasonal variability of the 800–730 hPa mean ω is complex. It is more pronounced at the lower levels, with ascent in March–April reduced to 70% of its annual mean at 802 hPa (Figure S2a), although this reduction is substantially stronger than in CSH6 (Figure 2). In the SH ITCZ, our estimates indicate that in March ω is strongest, even more than in the NH ITCZ around 800 hPa (Figures 2m–2o and S2a).

We find net vertical divergence in both ITCZs in the 800–730 hPa layer (Figures 2 and S2b), implying horizontal convergence, generally consistent with the other TRMM-based algorithms, but the reanalyses show divergence (Figure 2), associated with the overestimation of the depth of the shallow horizontal outflow up to 600–400 hPa (Figure 2), similar to idealized model simulations [*Nolan et al.*, 2007, 2010]. For the NH ITCZ, we find that the horizontal inflow in the 800–700 hPa layer contributes up to 60% of the ascending mass flux near 700 hPa in March–April, but this decreases to around 10% in July–November (Figures 2 and S2a). The former is substantially larger than in CSH6 and other TRMM algorithms, due to the smaller ω values near 800 hPa. On the other hand, the 800–730 hPa vertical divergence in the SH ITCZ is substantially smaller than in the NH in February–April (Figures 2m–2o and S2b).

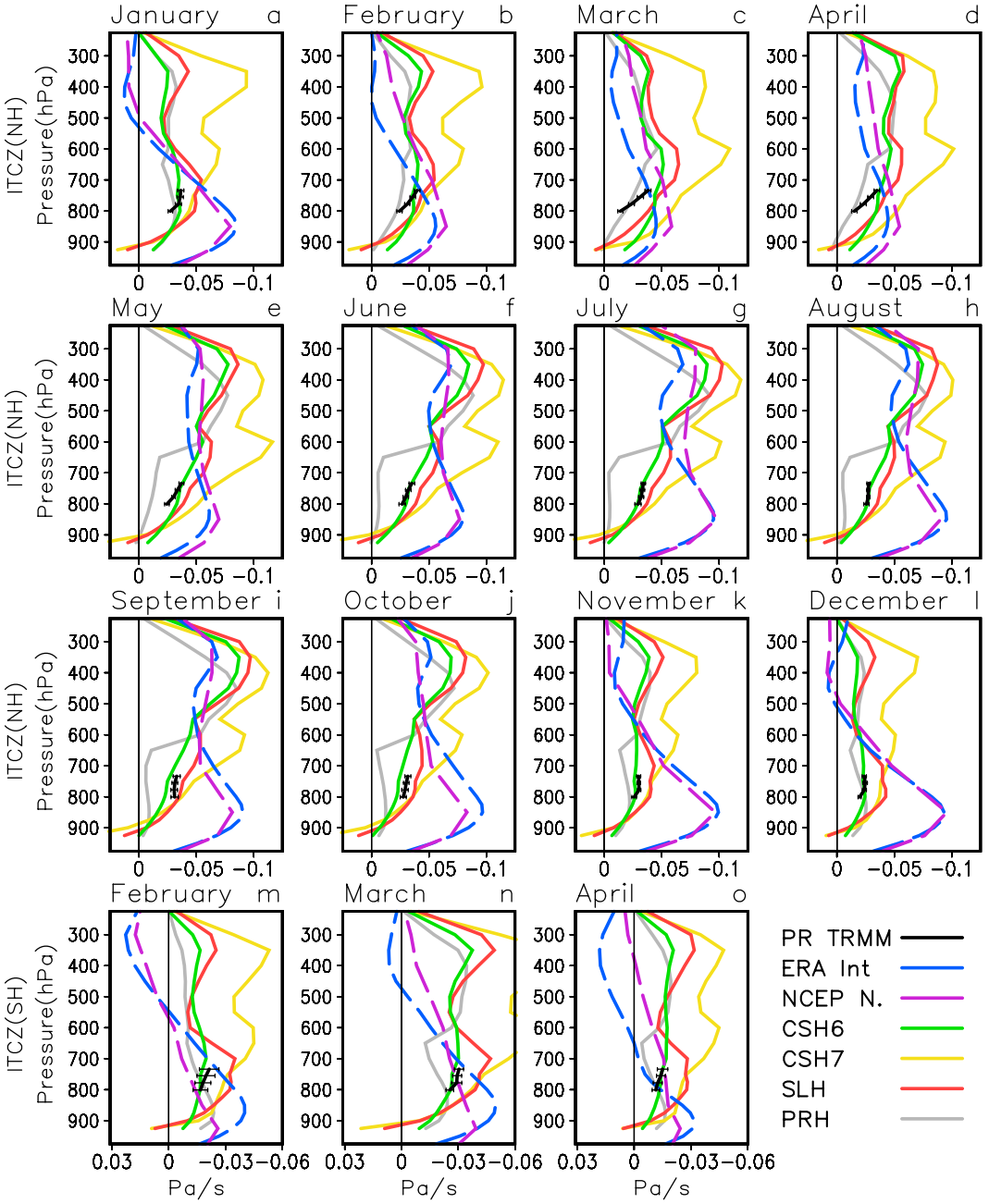

Figure 2. Monthly mean climatological (1998–2010) vertical pressure velocity (ω; Pa/s) profiles in the (a–l) NH and (m–o) SH eastern Pacific ITCZ (95°W–85°W) derived from TRMM 2A25 (this study; black bar indicates 1 standard error based on the 13 monthly values); from TRMM-based retrievals: CSH6 and CSH7 (green and yellow), SLH (red), PRH (grey); and from the ERA Interim and NCEP/NCAR reanalysis (blue and purple).

Although the reanalyses exaggerate the depth of the shallow ascent, its existence has been shown with in situ observations for the boreal fall [*Zhang et al.*, 2004]. This is clearly shown in our EPIC2001 ω estimate, which peaks near 870 hPa and is consistent with our TRMM PR estimate (Figure 3e). However, none of the other TRMM-based estimates shows this shallow peak for September–October 2001 (Figure 3e) or climatologically (Figures 2i and 2j), indicating that they are not reliable below 700 hPa in this region.

Our EPIC2001-based ω peak at 400 hPa was -0.12 ± 0.24 Pa/s, consistent with CSH6 (Figure 3e). This value is similar to the magnitude of the shallow peak and about twice as large as in the two reanalyses (Figure 3e). Although the uncertainty in our estimated is very large, the weight of the combined evidence supports

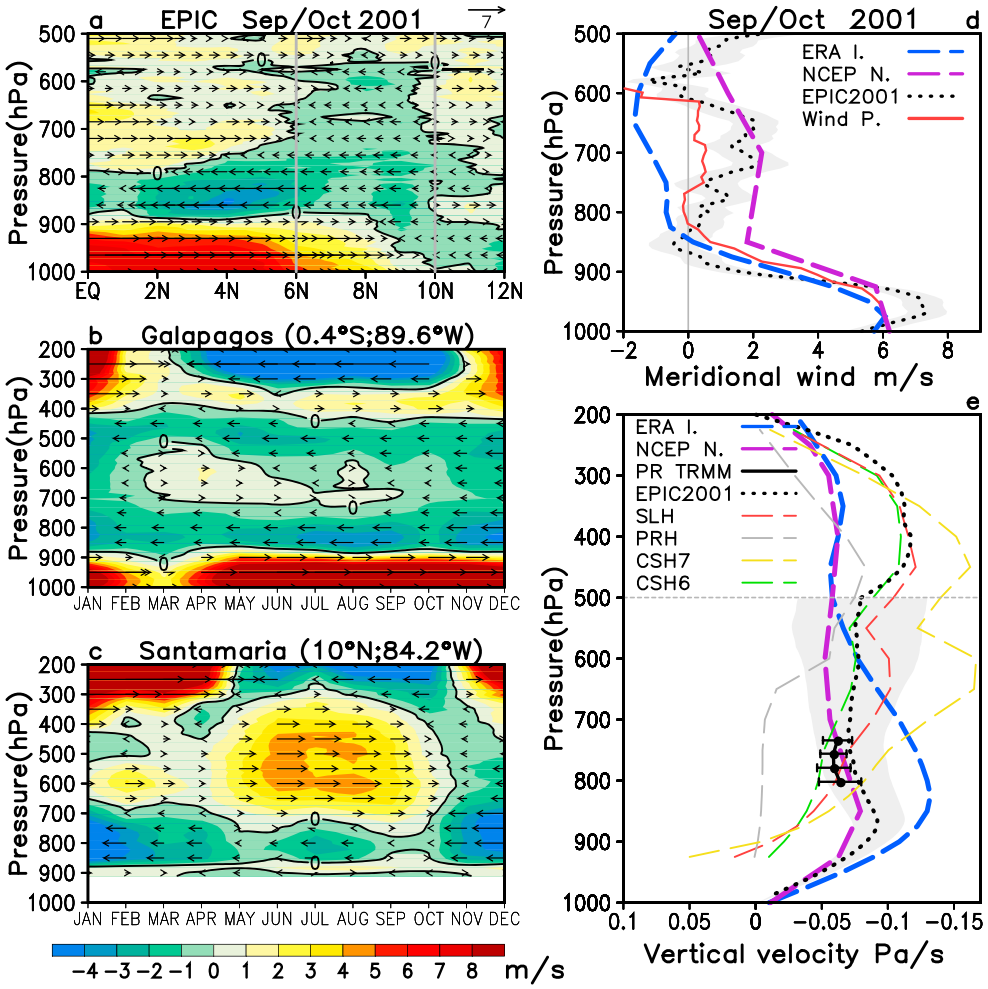

Figure 3. (a) Mean meridional wind (m/s) vertical section along 95°W in September–October 2001 during EPIC2001. Meridional wind (m/s) climatology from radiosondes at (b) Galápagos (1999–2015) and (c) Juan Santamaria (1999–2015). Mean September–October 2001 profiles of (d) near-equatorial meridional wind (m/s) and (e) vertical velocity in the NH ITCZ. Data are from TRMM 2A25 (with standard error, black solid), EPIC2001 dropsondes (black dotted, standard error in grey shading), the Galápagos wind profiler (red solid), NCEP/NCAR (purple dashed), ERA-Interim (blue dashed), and the SLH, PRH, CSH7, and CSH6 retrievals (red, grey, yellow, and green dashed).

the conclusion that the lower and upper tropospheric peaks in ω in the NH ITCZ during EPIC2001 were comparable.

3.2. Meridional Flow in Fall

During September–October, the surface meridional wind is southerly up to 10°N (Figures 1a and S3a), extending up to 900 hPa north of the equator (Figure 3a), probably somewhat deeper to the south (Figure S4a for November) and feature maximum surface net convergence in the ITCZ at 6°N and net divergence south of 4°N, maximizing slightly south of the equator (Figure S3b). Around 3°S, the surface meridional wind would lead to a convergence maximum, associated to the strong meridional sea surface temperature gradients around the cold tongue [*Wallace et al.*, 1989] but is canceled by the surface zonal divergence associated with the descending motion of the Walker circulation [*Wang and Enfield*, 2003], which also contributes to the equatorial divergence and weakens the NH ITCZ slightly (Figure S3b). Above the surface, in situ data show the shallow meridional circulation, with southerly surface trade winds converging in the ITCZ below ≈870 hPa, and northerly return flow at 800 hPa diverging from the ITCZ and reaching at least 8°S [*Zhang et al.*, 2004] (Figures 3a, 3b, and S4a).

At Galápagos, a southerly midlevel flow (SMF) is seen in the soundings around 700 hPa (Figure 3b) between March and September (750 and 550 hPa according to the wind profiler; not shown) but transitions to northerly

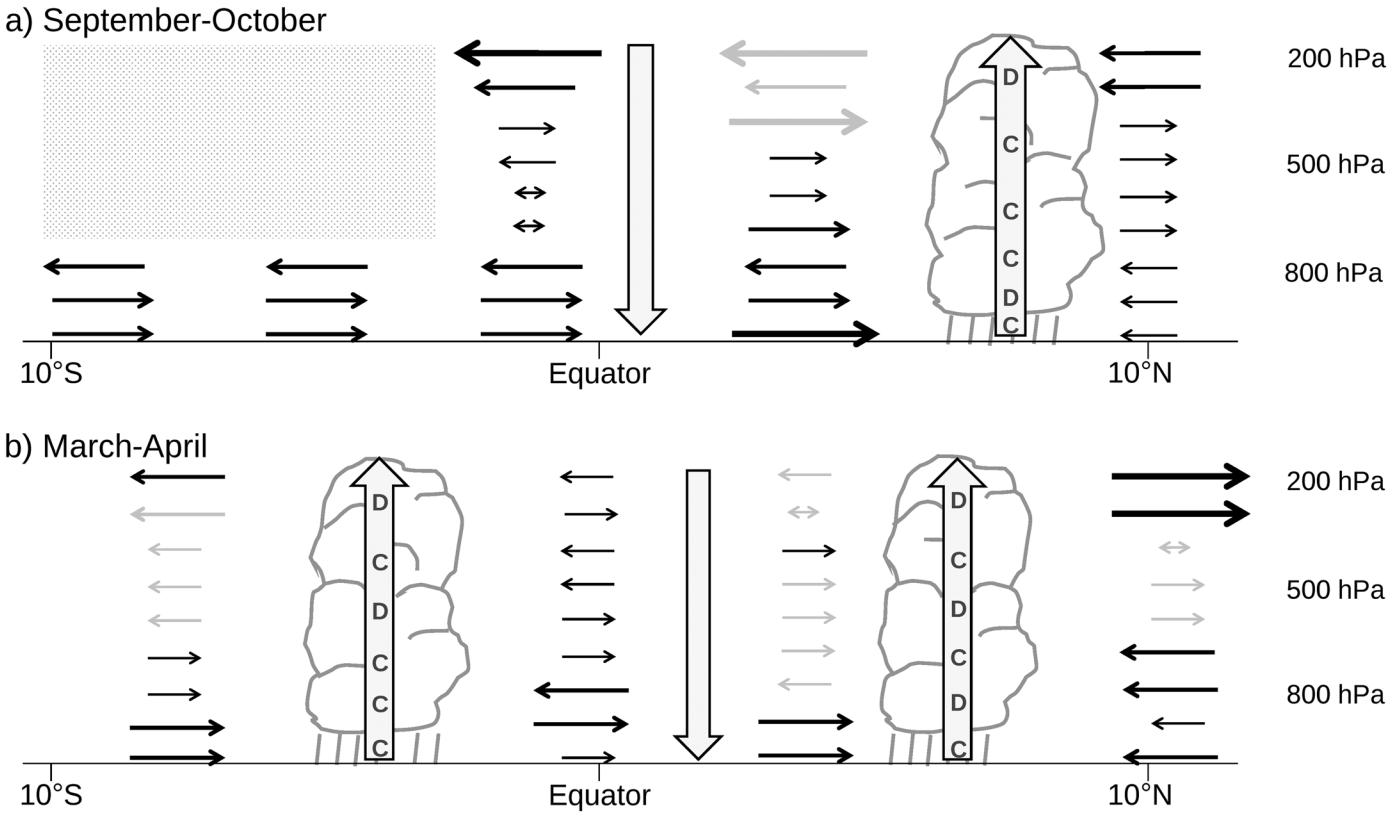

Figure 4. Sketch of the climatological meridional circulation in the eastern Pacific (95°–85°W) in (a) September–October and (b) March–April. Horizontal arrows indicate mean meridional wind (small: 0–2 m/s; medium: 2–6 m/s; large: >6 m/s; double headed: variable), with grey arrows and shading indicating weak observational constraint. (c and d) Horizontal convergence and divergence, respectively.

in October. During EPIC2001, the SMF was seen between 800 hPa to at least 500 hPa, reaching 6°N (Figure 3a) in six out of the eight flights. At that time, it was weaker in the Galápagos profiler than in the equatorial EPIC2001 soundings (Figure 3d). This suggests divergence of the equatorial subsidence at these levels [e.g., *Battisti and Ovens*, 1995] enhancing the SMF north of the equator. The model simulations of *Nolan et al.* [2007, 2010] indicate a "midlevel inflow" between 500 and 350 hPa, consistent with the strong horizontal convergence around 500–400 hPa in CSH6 (Figures 2i and 2j), although this is at higher altitude and stronger than the SMF, which is not simulated.

North of 10°N, EPIC2001 dropsondes (Figure 3a), Santamaria soundings (Figure 3c) and the pilot balloons in Liberia (not shown) indicate northerly trade surface winds up to 900 hPa, with southerly flow above, another northerly layer between 850 and 750 hPa, and southerlies up to 400 hPa. Above 350 hPa, soundings (Juan Santamaria, Figure 3c, and Acapulco, not shown) indicate northerly flow to the north of the ITCZ and near the equator (Galápagos; Figure 3b), while the horizontal divergence indicated by the CSH6 data (Figures 2i and 2j) at these levels imply strong northerly flow to the south of the ITCZ.

The Galápagos soundings indicate year-round southerly flow around 400–350 hPa and northerly flow around 550–400 hPa (Figure 3b). Further to the south, the November TAO soundings (Figure S4a) are the only other upper air wind data south of the equator, but their sparseness and the substantial synoptic-scale variability in the meridional wind associated with easterly [e.g., *Tai and Ogura*, 1987], eastward inertio-gravity, and mixed Rossby-gravity waves [e.g., *Wheeler and Kiladis*, 1999] limits their usefulness for estimating the mean flow.

Both reanalyses agree with our EPIC2001 ω estimate up to 900 hPa (NCEP-NCAR up to 750 hPa), indicating an adequate representation of the near-surface horizontal convergence (Figure 3e). However, they both exaggerate the extent of the horizontal divergence to at least 600 hPa (≈750 hPa in EPIC2001 and TRMM PR), indicating that surface flow alone might not be a strong constraint on low-level circulation [cf. *Handlos and Back*, 2014].

3.3. Meridional Flow in Spring

During March–April, the surface meridional winds are generally weaker, with southerlies extending to 6°N (Figure S3a). We find the ITCZs located around 5°S and 5°N, with a symmetric distribution of surface convergence relative to the equator, although precipitation is about twice as large in the northern ITCZ (Figures 1b and S3b). Zonal surface divergence is small, except north of 5°N (Figure S3b), associated with the fanning of the Papagayo gap wind [*Chelton et al.*, 2000a]), which is active during this period [*Xie et al.*, 2005]. The southerly surface trades around 8°S are limited to below 700 hPa, with maximum around 970 hPa, according to the TAO soundings, but becomes shallower (below 900 hPa) and weaker toward the equator (Figure S4b), consistent with the Galápagos radiosoundings (Figure 3b) and profiler (not shown).

The Galápagos meridional wind profiles (Figure 3b) have a complex structure, with northerly flow around 900–700 hPa and 500–400 hPa and southerly flow around 700–500 hPa (SMF) and 400–300 hPa, while at 200 hPa, the flow transitions from southerly (November–March) to northerly (April–October). The horizontal divergence around 200 hPa in the SH ITCZ indicated by CSH6 (Figures 2c and 2d) suggests southerly flow south of the ITCZ, consistent with the TAO soundings (Figure S4b). This is qualitatively consistent with the SH ITCZ structure in the double-ITCZ run by *Nolan et al.* [2010, Figure 7], except that the simulated meridional flow structure is shifted upward by 100–150 hPa.

Around 10°N, the low-level northerly flow is mainly associated with the Papagayo jet and, to a smaller extent, the Tehuantepec jet. The Papagayo jet is mostly zonal, with its core extending from the mountain gap around 11.5°N toward around 9°N, 95°W, from the surface to 600 hPa, with its core around 925–850 hPa (Figure S4d). The TAO soundings at 95°W show that Papagayo jet flows toward the ITCZ in the 800–600 hPa layer, while below 900 hPa the fanning or spreading out of the jet as it exits the gap [*Chelton et al.*, 2000a, 2000b] makes it enter ITCZ south of 10°N (Figure S4b). The splitting of the jet coincides approximately with the height of the topography around the gap [e.g., *Xu et al.*, 2005]. Since Santamaria station is at an altitude of 932 masl, only northerly flow between 880 and 700 hPa is seen, peaking between November and April (Figure 3c). At upper levels (300–200 hPa), the radiosoundings at Santamaria (Figure 3c) indicate southerly flow between November and April, approximately consistent with the TAO (Figure S4b) and Acapulco (not shown) soundings. At midlevels, the sounding data are less coherent, but at Santamaria there is southerly flow around 600–500 hPa (Figure 3c). Since CSH6 indicates horizontal convergence around 500–400 hPa (Figure 2cd), southerly flow could be expected south of the NH ITCZ, consistent with the TAO soundings (Figure S4b). On the other hand, the TRMM data indicate strong horizontal convergence between 800 and 700 hPa (Figures 2c and 2d), suggesting that the Papagayo jet does not exit but rather ascends in the ITCZ (Figure S4b).

4. Discussion

The results above indicate a complex structure of the meridional circulation in the eastern Pacific, which in the fall can be approximately described as two meridional cells vertically superposed [*Nolan et al.*, 2007, 2010] (Figure 4a), whereas in spring, the circulation has single-cell structures poleward of the two ITCZs, while just north of the equator the circulation shows some hints of the double cells (Figure 4b).

Our results warn that both model-based reanalysis or retrieval algorithms based on look-up tables are problematic for characterizing the convective circulation in this region. Although the EPIC2001 campaign was a crucial source of information for this study, it is necessary to implement more comprehensive and focused in situ observations. New satellite missions, such as Global Precipitation Measurement [*Smith et al.*, 2007], which can measure light rainfall and quantify solid precipitation, and the upcoming ADM-Aeolus [*European Space Agency et al.*, 2008], which will be able to measure wind profiles, will provide valuable information, but it will need to be validated. The diurnal cycle of precipitation [*Bain et al.*, 2010] and the meridional circulation [*Takahashi*, 2012] should also be taken in consideration. We believe that this region should be an important focus for the Tropical Pacific Observing System 2020 project [*OOPC*, 2014], as this could help hasten our advances toward identifying and correcting the origin of the pervasive double-ITCZ bias in climate models.

Acknowledgments

The data used in this paper were acquired from Goddard Earth System division and Information Service Center [TRMM and TRMM-based algorithms: CSH6 (product CSH), CSH7 (product 3H31), and SLH (product 3H25); http://disc.sci.gsfc.nasa.gov/], ECMWF (ERA Interim reanalysis; http://apps.ecmwf.int/datasets/), NOAA/ESRL (NCEP-NCAR reanalysis and wind profiler; http://www.esrl.noaa.gov/psd/), Centre de Recherche et d'Exploitation Satellitaire at IFREMER (QuikSCAT; http://cersat.ifremer.fr/data/products), PACS SONET project (pilot balloons; http://nssl.noaa.gov/projects/pacs/web/), University of Wyoming (radiosoundings; http://weather.uwyo.edu/), and TAO Project Office of NOAA/PMEL (TAO buoys; http://pmel.noaa.gov/tao/). We also thank to S. de Szoeke, M. Katsumata, and C. Fairall for providing the EPIC2001, PRH, and TAO radiosounding data, respectively. We also appreciate the help of NASA-GSFC-PPS team and S. Shige. In addition, we thank G. Kiladis for useful discussions and comments and an anonymous reviewer for his/her comments. This study was supported by the PPR 068 "Reducción de Vulnerabilidad y Atención de Emergencias por Desastres" and the project "Impacts of Climate Variability and Climate Change on the Mangrove Ecosystem in Tumbes, Peru" (IDRC 106714).

References

Back, L. E., and C. S. Bretherton (2006), Geographic variability in the export of moist static energy and vertical motion profiles in the tropical Pacific, *Geophys. Res. Lett.*, *33*, L17810, doi:10.1029/2006GL026672.

Back, L. E., and C. S. Bretherton (2009), On the relationship between SST gradients, boundary layer winds, and convergence over the tropical oceans, *J. Clim.*, *22*(15), 4182–4196.

Bain, C. L., G. Magnusdottir, P. Smyth, and H. Stern (2010), Diurnal cycle of the Intertropical Convergence Zone in the east Pacific, *J. Geophys. Res.*, *115*, D23116, doi:10.1029/2010JD014835.
Battisti, D. S., and D. D. Ovens (1995), The dependence of the low-level equatorial easterly jet on Hadley and Walker circulations, *J. Atmos. Sci.*, *52*(22), 3911–3931.
Bellucci, A., S. Gualdi, and A. Navarra (2010), The double-ITCZ syndrome in coupled general circulation models: The role of large-scale vertical circulation regimes, *J. Clim.*, *23*(5), 1127–1145.
Chelton, D. B., M. H. Freilich, and S. Esbensen (2000a), Satellite observations of the wind jets off the Pacific coast of Central America. Part I: Case studies and statistical characteristics, *Mon. Weather Rev.*, *128*, 1993–2018.
Chelton, D. B., M. H. Freilich, and S. Esbensen (2000b), Satellite observations of the wind jets off the Pacific coast of Central America. Part II: Regional relationships and dynamical considerations, *Mon. Weather Rev.*, *128*, 2019–2043.
Cronin, M. F., N. Bond, C. Fairall, J. Hare, M. J. McPhaden, and R. A. Weller (2002), Enhanced oceanic and atmospheric monitoring underway in eastern Pacific, *Eos Trans. AGU*, *83*(19), 205–216.
de Szoeke, S. P., C. S. Bretherton, N. A. Bond, M. F. Cronin, and B. M. Morley (2005), EPIC 95 W observations of the eastern Pacific atmospheric boundary layer from the cold tongue to the ITCZ, *J. Atmos. Sci.*, *62*(2), 426–442.
de Szoeke, S. P., and S. P. Xie (2008), The tropical eastern Pacific seasonal cycle: Assessment of errors and mechanisms in IPCC AR4 coupled ocean-atmosphere general circulation models, *J. Clim.*, *21*, 2573–2590.
Dee, D. P., et al. (2011), The ERA-Interim reanalysis: Configuration and performance of the data assimilation system, *Q. J. R. Meteorol. Soc.*, *137*, 553–597, doi:10.1002/qj.828.
European Space Agency, E. Andersson, and P. Clissold (2008), ADM-Aeolus: Science Report. ESA Communication Production Office. [Available at http://esamultimedia.esa.int/docs/SP-1311_ADM-Aeolus_FINAL_low-res.pdf.]
Flato, G., et al. (2013), *Evaluation of Climate Models—Climate Change 2013: The Physical Science Basis; Contribution of Working Group I to the Fifth Assessment Report of the Intergovernmental Panel on Climate Change,* edited by T. F. Stocker et al., Cambridge Univ. Press, Cambridge, U. K., and New York.
Gentemann, C. L., F. J. Wentz, C. A. Mears, and D. K. Smith (2004), In situ validation of Tropical Rainfall Measuring Mission microwave sea surface temperatures, *J. Geophys. Res.*, *109*, C04021, doi:10.1029/2003JC002092.
Gu, G., R. F. Alder, and A. H. Sobel (2005), The eastern Pacific ITCZ during the boreal spring, *J. Atmos. Sci.*, *62*(4), 1157–1174.
Halpern, D., and C.-H. Hung (2001), Satellite observations of the southeast Pacific intertropical convergence zone during 1993–1998, *J. Geophys. Res.*, *106*(D22), 28,107–28,112.
Handlos, Z. J., and L. E. Back (2014), Estimating vertical motion profile shape within tropical weather states over the oceans, *J. Clim.*, *27*(20), 7667–7686.
Hartten, L. M., and K. S. Gage (2000), ENSO's impact on the annual cycle: The view from Galápagos, *Geophys. Res. Lett.*, *27*(3), 385–388.
Hastenrath, S. (2002), The intertropical convergence zone of the eastern Pacific revisited, *Int. J. Climatol.*, *22*(3), 347–356.
Houze, R. A. (1989), Observed structure of mesoscale convective systems and implications for large-scale heating, *Q. J. R. Meteorol. Soc.*, *115*(487), 425–461.
Huffman, G. J., D. T. Bolvin, E. J. Nelkin, D. B. Wolff, R. F. Adler, G. Gu, Y. Hong, K. Bowman, and E. F. Stocker (2007), The TRMM Multisatellite Precipitation Analysis (TMPA): Quasi-global, multiyear, combined-sensor precipitation estimates at fine scales, *J. Hydrometeorol.*, *8*(1), 38–55.
Iguchi, T., T. Kozu, R. Meneghini, J. Awaka, and K. I. Okamoto (2000), Rain-profiling algorithm for the TRMM Precipitation Radar, *J. Appl. Meteorol.*, *39*(12), 2038–2052.
Janowiak, J. E., A. Gruber, C. R. Kondragunta, R. E. Livezey, and G. J. Huffman (1998), A comparison of the NCEP-NCAR reanalysis precipitation and the GPCP rain gauge-satellite combined dataset with observational error considerations, *J. Clim.*, *11*(11), 2960–2979.
JAXA, and NASA (2011), Tropical rainfall measuring mission (TRMM) precipitation radar algorithm. Instruction manual for version 7. [Available at http://www.eorc.jaxa.jp/TRMM/documents/PR_algorithm_product_information/pr_manual/PR_Instruction_Manual_V7_L1.pdf.]
Kalnay, E., et al. (1996), The NCEP/NCAR 40-year reanalysis project, *Bull. Am. Meteorol. Soc.*, *77*(3), 437–471.
Kistler, R., et al. (2001), The NCEP-NCAR 50-year reanalysis: Monthly means CD-ROM and documentation, *Bull. Am. Meteorol. Soc.*, *82*(2), 247–267.
Kodama, Y. M., M. Katsumata, S. Mori, S. Satoh, Y. Hirose, and H. Ueda (2009), Climatology of warm rain and associated latent heating derived from TRMM PR observations, *J. Clim.*, *22*(18), 4908–4929.
Kummerow, C., W. Barnes, T. Kozu, J. Shiue, and J. Simpson (1998), The Tropical Rainfall Measuring Mission (TRMM) sensor package, *J. Atmos. Oceanic Technol.*, *15*(3), 809–817.
Lietzke, C. E., C. Deser, and T. H. Vonder Haar (2001), Evolutionary structure of the eastern Pacific double ITCZ based on satellite moisture profile retrievals, *J. Clim.*, *14*(5), 743–751.
Lin, J. L. (2007), The double-ITCZ problem in IPCC AR4 coupled GCMs: Ocean-atmosphere feedback analysis, *J. Clim.*, *20*(18), 4497–4525.
Ma, C. C., C. R. Mechoso, A. W. Robertson, and A. Arakawa (1996), Peruvian stratus clouds and the tropical Pacific circulation: A coupled ocean-atmosphere GCM study, *J. Clim.*, *9*(7), 1635–1645.
Mechoso, C. R., et al. (1995), The seasonal cycle over the tropical Pacific in coupled ocean-atmosphere general circulation models, *Mon. Weather Rev.*, *123*(9), 2825–2838.
Nolan, S. D., C. Zhang, and S.-H. Chen (2007), Dynamics of the shallow circulation around ITCZ regions, *J. Atmos. Sci.*, *64*(7), 2262–2285.
Nolan, S. D., S. Powell, and B. Mapes (2010), Idealized simulations of the Intertropical Convergence Zone and its multilevel flows, *J. Atmos. Sci.*, *67*(12), 4028–4053.
OOPC (2014), *Report of the Tropical Pacific Observation System 2020 (TPOS 2020) Workshop, Volume 1: Workshop Report and Recommendations*, 66 pp., GCOS-184/GOOS-205/WCRP-6/2014. [Available at http://www.wmo.int/pages/prog/gcos/Publications/gcos-184_II.pdf.]
Oueslati, B., and G. Bellon (2015), The double ITCZ bias in CMIP5 models: Interaction between SST, large-scale circulation and precipitation, *Clim. Dyn.*, *44*(3–4), 585–607.
Philander, S. G. H., D. Gu, G. Lambert, T. Li, D. Halpern, N. C. Lau, and R. C. Pacanowski (1996), Why the ITCZ is mostly north of the equator, *J. Clim.*, *9*(12), 2958–2972.
Raymond, D. J., S. K. Esbensen, C. Paulson, M. Gregg, C. S. Bretherton, W. A. Petersen, R. Cifelli, L. K. Shay, C. Ohlmann, and P. Zuidema (2004), EPIC2001 and the coupled ocean-atmosphere system of the tropical east Pacific, *Bull. Am. Meteorol. Soc.*, *85*(9), 1341–1354.
Ricciardulli, L., and F. Wentz (2011), Reprocessed QuikSCAT (V04) wind vectors with Ku-2011 geophysical model function, *Remote Sens. Syst. Tech. Rep. 43011(8)*.

Satoh, S., A. Noda, and T. Iguchi (2001), Retrieval of latent heating profiles from TRMM radar data, in *The 30th Conference on Radar Meteorology*, pp. 340–342, Am. Meteorol. Soc., Munich, Germany.
Schumacher, C., R. A. Houze, and I. Kraucunas (2004), The tropical dynamical response to latent heating estimates derived from the TRMM Precipitation Radar, *J. Atmos. Sci.*, *61*(12), 1341–1358.
Serra, Y., and M. J. McPhaden (2003), Multiple time- and space-scale comparisons of ATLAS buoy rain gauge measurements with TRMM satellite precipitation measurements, *J. Appl. Meteorol.*, *42*, 1045–1059.
Shige, S., Y. N. Takayabu, W. K. Tao, and D. E. Johnson (2004), Spectral retrieval of latent heating profiles from TRMM PR data. Part I: Development of a model-based algorithm, *J. Appl. Meteorol.*, *43*(8), 1095–1113.
Shige, S., Y. N. Takayabu, W. K. Tao, and C. L. Shie (2007), Spectral retrieval of latent heating profiles from TRMM PR data. Part II: Algorithm improvement and heating estimates over tropical ocean regions, *J. Appl. Meteorol. Climatol.*, *46*(7), 1098–1124.
Short, D. A., and K. Nakamura (2000), TRMM radar observations of shallow precipitation over the tropical oceans, *J. Clim.*, *13*(23), 4107–4124.
Smith, E. A., et al. (2007), International Global Precipitation Measurement (GPM) program and mission: An overview, in *Measuring Precipitation From Space*, pp. 611–653, Springer, Netherlands.
Takahashi, K. (2012), Thermotidal and land-heating forcing of the diurnal cycle of oceanic surface winds in the eastern tropical Pacific, *Geophys. Res. Lett.*, *39*, L04805, doi:10.1029/2011GL050692.
Takahashi, K., and D. S. Battisti (2007), Processes controlling the mean tropical Pacific precipitation pattern. Part I: The Andes and the eastern Pacific ITCZ, *J. Clim.*, *20*, 3434–3451.
Tai, K.-S., and Y. Ogura (1987), An observational study of easterly waves over the eastern Pacific in the northern summer using FGGE data, *J. Atmos. Sci.*, *44*(2), 339–361.
Tao, W.-K., et al. (2001), Retrieved vertical profiles of latent heat release using TRMM rainfall products for February 1998, *J. Appl. Meteorol.*, *40*(6), 957–982.
Tao, W. K., et al. (2006), Retrieval of latent heating from TRMM measurements, *Bull. Am. Meteorol. Soc.*, *87*(11), 1555–1572.
Tao, W. K., S. Lang, X. Zeng, S. Shige, and Y. Takayabu (2010), Relating convective and stratiform rain to latent heating, *J. Clim.*, *23*(7), 1874–1893.
Wallace, J. M., T. P. Mitchell, and C. Deser (1989), The influence of sea-surface temperature on surface wind in the eastern equatorial Pacific: Seasonal and interannual variability, *J. Clim.*, *2*(12), 1492–1499.
Wang, C., and D. B. Enfield (2003), A further study of the tropical western hemisphere warm pool, *J. Clim.*, *16*, 1476–1493.
Wang, C. (2004), ENSO, Atlantic climate variability, and the Walker and Hadley circulations, in *The Hadley Circulation: Present, Past and Future*, pp. 173–202, Springer, Netherlands.
Wheeler, M. C., and G. N. Kiladis (1999), Convectively coupled equatorial waves: Analysis of clouds and temperature in the wavenumber-frequency domain, *J. Atmos. Sci.*, *56*, 374–398.
Wu, R., and S. P. Xie (2003), On equatorial Pacific surface wind changes around 1977: NCEP-NCAR reanalysis versus COADS observations, *J. Clim.*, *16*(1), 167–173.
Xie, S. P., and S. G. H. Philander (1994), A coupled ocean-atmosphere model of relevance to the ITCZ in the eastern Pacific, *Tellus A*, *46*(4), 340–350.
Xie, S.-P. (1996), Westward propagation of latitudinal asymmetry in a coupled ocean-atmosphere model, *J. Atmos. Sci.*, *53*, 3236–3250.
Xie, S.-P., H. Xu, W. S. Kessler, and M. Nonaka (2005), Air-sea interaction over the eastern Pacific warm pool: Gap winds, thermocline dome, and atmospheric convection, *J. Clim.*, *18*(1), 5–20.
Xu, H., S. P. Xie, Y. Wang, and R. J. Small (2005), Effects of Central American mountains on the eastern Pacific winter ITCZ and moisture transport, *J. Clim.*, *18*, 3856–3873.
Yin, B., and B. A. Albrecht (2000), Spatial variability of atmospheric boundary layer structure over the eastern equatorial Pacific, *J. Clim.*, *13*(9), 1574–1592.
Zhang, C. (2001), Double ITCZs, *J. Geophys. Res.*, *106*(D11), 11,785–11,792.
Zhang, C., M. McGauley, and N. A. Bond (2004), Shallow meridional circulation in the tropical eastern Pacific, *J. Clim.*, *17*(1), 133–139.
Zhang, C., D. S. Nolan, C. D. Thorncroft, and H. Nguyen (2008), Shallow meridional circulations in the tropical atmosphere, *J. Clim.*, *21*(14), 3453–3470.
Zhang, X., H. Liu, and M. Zhang (2015), Double ITCZ in coupled ocean-atmosphere models: From CMIP3 to CMIP5, *Geophys. Res. Lett.*, *42*, 8651–8659, doi:10.1002/2015GL065973.